Breather gas fission from elliptic potentials in self-focusing media

Gino Biondini,[1,2] Gennady A. El,[3] Xu-Dan Luo,[4] Jeffrey Oregero,[5] and Alexander Tovbis[6]

[1]*Department of Mathematics, State University of New York at Buffalo, Buffalo, New York 14260, USA*
[2]*Department of Physics, State University of New York at Buffalo, Buffalo, New York 14260, USA*
[3]*Department of Mathematics, Physics and Electrical Engineering, Northumbria University, Newcastle upon Tyne NE1 8ST, United Kingdom*
[4]*Academy of Mathematics and Systems Science, Chinese Academy of Sciences, Beijing 100190, China*
[5]*Department of Mathematics, University of Kansas, Lawrence, Kansas 66045, USA*
[6]*Department of Mathematics, University of Central Florida, Orlando, Florida 32816, USA*

(Received 24 July 2024; accepted 26 November 2024; published 6 January 2025)

We present an analytical model of integrable turbulence in the focusing nonlinear Schrödinger (fNLS) equation, generated by a one-parameter family of finite-band elliptic potentials in the semiclassical limit. We show that the spectrum of these potentials exhibits a thermodynamic band/gap scaling compatible with that of soliton and breather gases depending on the value of the elliptic parameter m of the potential. We then demonstrate that, upon augmenting the potential by a small random noise (which is inevitably present in real physical systems), the solution of the fNLS equation evolves into a fully randomized, spatially homogeneous breather gas, a phenomenon we call breather gas fission. We show that the statistical properties of the breather gas at large times are determined by the spectral density of states generated by the unperturbed initial potential. We analytically compute the kurtosis of the breather gas as a function of the elliptic parameter m, and we show that it is greater than 2 for all nonzero m, implying non-Gaussian statistics. Finally, we verify the theoretical predictions by comparison with direct numerical simulations of the fNLS equation. These results establish a link between semiclassical limits of integrable systems and the statistical characterization of their soliton and breather gases.

DOI: 10.1103/PhysRevE.111.014204

I. INTRODUCTION

The focusing nonlinear Schrödinger (fNLS) equation is a ubiquitous model describing nonlinear wave propagation arising in a variety of physical settings, including deep water waves [1], optics [2], plasmas [3], and Bose-Einstein condensates (BECs) [4]. The fNLS equation is also a completely integrable infinite-dimensional Hamiltonian system [5–10], endowed with a deep mathematical structure, including the existence of infinite families of exact solutions with both zero and nonzero background describing the elastic interactions of N solitons. In addition, its initial value problem can in some cases be solved by the inverse scattering transform (IST) [11–19]. The formulation of the IST is based on the representation of the nonlinear evolution equation as the compatibility condition of two linear equations called a Lax pair. The first half of the Lax pair of the fNLS equation, namely the Zakharov-Shabat (ZS) scattering problem, is equivalent to an eigenvalue problem for a non-self-adjoint one-dimensional Dirac operator.

While the classical theory and applications of the fNLS equation are mostly concerned with the description of regular, deterministic wave structures, the inherent statistical nature of some physical wave phenomena in focusing media (e.g., rogue wave emergence) calls for the study of stochastic fNLS solutions, characterized in terms of the probability density function, correlation function, etc. Establishing a connection between the IST spectra of random fNLS solutions and their statistical properties in physical space represents a challenging problem, which has recently been formulated in the context of *integrable turbulence* [20,21]—the general theoretical framework for the description of a broad spectrum of stochastic wave phenomena in physical systems modeled by integrable equations. A particular type of integrable turbulence, termed *soliton gas* (SG), has recently attracted considerable attention [22,23] due to its appearance in many physical systems including water waves [24–27], nonlinear optics [28–30], and BECs [31,32]. Notably, SG dynamics has been shown to underpin some fundamental physical phenomena such as spontaneous modulational instability [33] and the rogue wave emergence [34] in focusing media.

The concept of a SG was introduced in Ref. [35] as an infinite collection of randomly distributed solitons with small spatial density and with a certain amplitude distribution. Soliton interactions, accompanied by well-defined phase shifts, result in a modification of the effective velocity of a "tracer" soliton in a gas over large propagation distances, enabling an approximate description of the emergent, large-scale hydrodynamics or kinetics of a weakly nonuniform/nonequilibrium SG. The kinetic description of a SG was generalized in Ref. [36] to a dense SG using finite-gap theory, and a general phenomenological construction of SG kinetic equation for a broad class of integrable systems was proposed in Ref. [37]. A systematic spectral theory of fNLS SGs was developed in Ref. [38], where it was also extended to the case of a SG on a nonzero background, i.e., a *breather gas* (BG). For recent advances on the spectral theory of soliton and breather gases and its relation to the generalized hydrodynamics of integrable

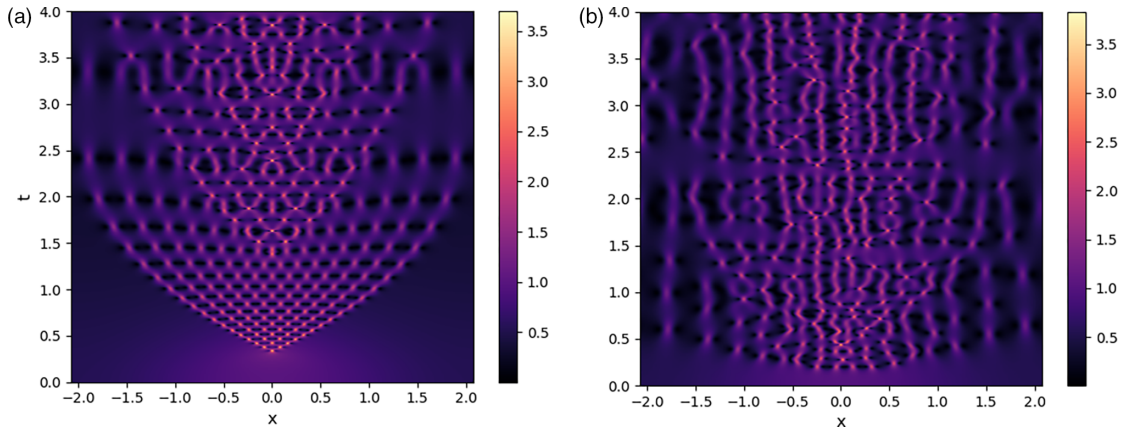

FIG. 1. Density plots of the time evolution of the potential in Eq. (4) according to fNLS equation (1) with $\epsilon = 1/20$, $m = 0.7$, and (a) without noise, (b) with zero-mean white Gaussian noise with standard deviation $\sigma = 10^{-2}$. In both cases, the spatial window was taken to be the period of the IC.

many-body classical and quantum systems, see Ref. [23]. For further rigorous analysis of SGs and BGs of the fNLS equation, including periodic SGs and BGs, see Ref. [39].

While BGs represent a natural generalization of SGs, possible mechanisms for their generation have remained largely unexplored. In this work we present an analytically tractable model of BG generation via fission, based on the semiclassical limit of the fNLS equation with initial data in the form of a periodic elliptic "dn" potential with elliptic parameter $m \in [0, 1]$, augmented by a small random noise. It was shown in Ref. [40] that the ZS spectrum of such elliptic potentials can be characterized analytically. It was also shown in Ref. [39] that, in the semiclassical limits, one hump, nonnegative, periodic potentials [including the Jacobi elliptic "dn" potential] are compatible with the so-called thermodynamic spectral scaling [38] and give rise to bound-state SGs or BGs. The addition of a small noise to the initial condition (IC) facilitates the "phase mixing" of the finite-gap semiclasical dn potential, giving rise, in the long-time limit, to a spatially uniform and statistically stationary integrable turbulence, associated with a BG (cf. Fig. 1).

The fundamental property of long-time effective "thermalization," or relaxation to a statistically stationary state, in an integrable system was established numerically in several scenarios of the evolution of random waves in the fNLS equation [41–43]. Here we extend this result to the qualitatively new framework of the BG fission, which encompasses a broad range of scenarios of transition to stationary integrable turbulence depending on the value of m in the semiclassical elliptic potential: from the nonlinear development of the spontaneous modulational instability for $m \to 0$ to the rarefied soliton gas fission for $m \to 1$. When the noise is sufficiently small, the ZS spectrum remains essentially unchanged from that of the semiclassical elliptic potential. The isospectrality of the BG fission enables one to take advantage of the results of Ref. [21] and evaluate statistical measures of the BG, such as the mean intensity and kurtosis, in terms of the spectral density of states of the initial elliptic potential. In Ref. [21], it was predicted that the kurtosis doubles in the long-time fNLS fission of the so-called partially coherent waves into a SG. Here we show analytically that this result generalizes to the BG fission from semiclassical elliptic potentials, and we confirm our results by comparison with direct numerical simulations of the time evolution of the noise-augmented potential.

An important ingredient of our construction is the interpretation of a BG as a "composite SG" comprising of two spectrally distinct components: a regular SG and a *soliton condensate*, defined as a critically dense SG [38] and describing the modulationally unstable background in a BG. This composite SG provides a natural extension of the "pure" fNLS soliton condensate framework used in Refs. [33,44] to model the development of spontaneous (noise-induced) modulational instability of fNLS plane wave and genus one elliptic solutions.

II. NLS WITH DN POTENTIAL

The cubic fNLS equation is, in normalized and dimensionless form and in the semiclassical scaling,

$$i\epsilon q_t + \epsilon^2 q_{xx} + 2|q|^2 q = 0, \tag{1}$$

where subscripts x and t denote partial differentiation, $q(x, t)$ describes a complex-valued envelope of oscillations, and the physical meaning of the variables x and t varies depending on the physical context. (For example, in nonlinear fiber optics, x is a retarded time and t is the propagation distance through the medium.) Equation (1) is the compatibility condition $\mathbf{v}_{xt} = \mathbf{v}_{tx}$ of its Lax pair, namely the overdetermined linear system

$$\epsilon \mathbf{v}_x = (-iz\sigma_3 + Q)\,\mathbf{v}, \quad \epsilon \mathbf{v}_t = P\,\mathbf{v}, \tag{2}$$

for $\mathbf{v}(x, t, z) = (v_1, v_2)^T$, with $P = -2iz^2\sigma_3 + i(|q|^2 + Q_x)\,\sigma_3 - 2zQ$, where $\sigma_3 = \mathrm{diag}(1, -1)$ is the third Pauli matrix, and

$$Q(x, t) = \begin{pmatrix} 0 & q \\ -q^* & 0 \end{pmatrix}, \tag{3}$$

the asterisk denoting complex conjugate. The first half of Eq. (2) is the ZS scattering problem, and q and z are referred to respectively as the potential and the scattering parameter, or eigenvalue, since the first half of Eq. (2) can be rewritten as the eigenvalue problem $\mathcal{L}\mathbf{v} = z\mathbf{v}$, where $\mathcal{L} := i\sigma_3(\epsilon\partial_x - Q)$ is a one-dimensional Dirac operator.

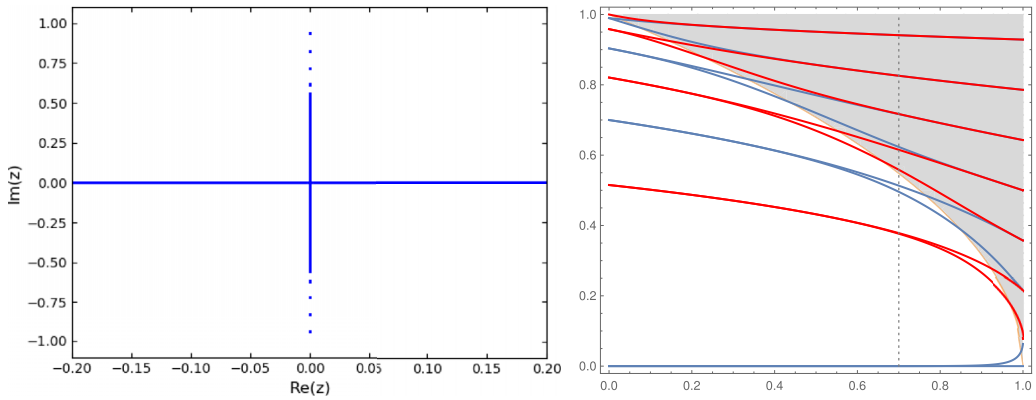

FIG. 2. Left: The spectrum of the dn potential (4) in the complex z plane with $m = 0.7$ for $\epsilon = 1/7$. Right: Periodic (red) and antiperiodic (blue) eigenvalues (vertical axis) as a function of the elliptic parameter m in $(0, 1)$ (horizontal axis) for $\epsilon = 1/7$. For every fixed value of m, as $\epsilon \to 0$, the number of bands grows like $1/\epsilon$. The yellow line separates the range $\Gamma_o = (0, iq_{\min})$ (in white) from the range $\Gamma_g = (iq_{\min}, iq_{\max})$ (in gray). The dashed line shows the value $m = 0.7$ corresponding to the spectrum in the left panel. For each fixed value of m, inside $z \in \Gamma_g$ the band widths decrease exponentially in ϵ, giving rise to point spectrum in the limit $\epsilon \to 0$. Conversely, inside Γ_o the band widths decrease only algebraically, giving rise to a continuous band in the limit $\epsilon \to 0$.

In Ref. [40] we characterized the Lax spectrum $\Sigma(\mathcal{L})$ of the above ZS problem with the potential

$$q(x, 0) = \mathrm{dn}(x; m), \quad x \in \mathbb{R}, \tag{4}$$

where $\mathrm{dn}(x; m)$ is a Jacobi elliptic function [45,46] and $m \in (0, 1)$ is the elliptic parameter. (Recall that the Lax spectrum $\Sigma(\mathcal{L})$ is defined as the set of values $z \in \mathbb{C}$ such that the focusing ZS scattering problem admits solutions $\mathbf{v}(x, z)$ that are bounded for all $x \in \mathbb{R}$.) Note the spatial period is $2L = 2K_m$, where $K_m = K(m)$ is the complete elliptic integral of first kind.

Two distinguished limiting cases are $m = 0, 1$. The case $m = 0$ reduces to the constant potential $q(x, 0) \equiv 1$, which is solved trivially, and for which $\Sigma(\mathcal{L}) = \mathbb{R} \cup [-i, i]$. Conversely, as $m \to 1$, $q(x, 0) \to \mathrm{sech}\ x$ and $K_m \to \infty$. This problem was studied in Ref. [47], where it was shown that $\Sigma(\mathcal{L})$ comprises the real z axis plus a set of purely imaginary discrete eigenvalues uniformly distributed in the interval $(-i, i)$. Moreover, it was shown that $\mathrm{sech}\ x$ is a reflectionless potential (giving rise to pure soliton solutions) if and only if $\epsilon = 1/N$, with $N \in \mathbb{N}$. This work connects these two limiting cases by characterizing the class of periodic potentials (4) for all $0 < m < 1$. Figure 1 shows for $\epsilon = 1/20$ and $m = 0.7$ the time evolution of the dn potential according to fNLS without noise (left), and with Gaussian noise (right).

The structure of the Lax spectrum can be studied via Bloch-Floquet theory using the monodromy matrix $M(z) = \Phi^{-1}(x, z)\Phi(x + 2L, z)$, where $\Phi(x, z)$ is a fundamental matrix solution of the scattering problem, and $2L$ is the minimal period of the potential. [Since $\Sigma(\mathcal{L})$ is invariant when the potential $q(x, t)$ evolves in time according to the fNLS Eq. (1), we will often omit the time dependence from all quantities below.] In turn, the Floquet discriminant is defined by $\Delta(z) = \mathrm{tr}\, M(z)/2$. Bounded solutions of the scattering problem then exist for $z \in \mathbb{C}$ such that $\mathrm{Im}\, \Delta(z) = 0$ and $-1 \leqslant \mathrm{Re}\, \Delta(z) \leqslant 1$. Importantly, $\Delta(z)$ is an entire function of z that is also Schwarz-symmetric: $\Delta(z^*) = \Delta^*(z)$. As a result, it is sufficient to consider the upper half plane, $\mathrm{Im}\, z \geqslant 0$. Since $\mathcal{L}$ is non-self-adjoint, $\Sigma(\mathcal{L})$ is not confined to the real z axis. Nonetheless, the zero-level curves of $\mathrm{Im}\, \Delta(z)$ define a countable set of analytic arcs Γ_n. Along each arc, the requirement $-1 \leqslant \mathrm{Re}\, \Delta(z) \leqslant 1$ then defines a spectral band. With these definitions, one can talk about bands as in a self-adjoint problem, the difference being that in the non-self-adjoint case the bands are not restricted to lie along the real z axis, but lie instead along the Γ_n.

The endpoints of the bands are periodic and antiperiodic eigenvalues of $\mathcal{L}$, namely, the values z for which $\Delta(z) = \pm 1$, which give rise to periodic and antiperiodic eigenfunctions, respectively. Moreover, the real z axis is an infinitely long band, and any band that intersects the real z axis transversally is called a "spine." Any potential whose spectrum is comprised of a finite number of bands is called a "finite-band" potential [8,9,48]. These special potentials correspond to the finite-genus solutions of all equations in the Ablowitz-Kaup-Newell-Segur (AKNS) hierarchy.

In Ref. [40] it was proved that for the dn potential (4) and $\epsilon = 1/N$, $N \in \mathbb{N}$, the Lax spectrum of the ZS scattering problem comprises $2N$ Schwarz-symmetric bands along the interval $(-i, i)$, and produces a genus $2N - 1$ solution of the fNLS equation (see Ref. [40] and the Appendix for details).

III. SEMICLASSICAL LIMIT AND BREATHER GAS

The spectrum of the dn potential (4) in the complex z plane for for $m = 0.7$ and $\epsilon = 1/7$. is shown in Fig. 2(left). Figure 2(right) shows, as a function of the elliptic parameter m (horizontal axis), the location of the periodic eigenvalues (red curves) and antiperiodic eigenvalues (blue curves) along the imaginary z axis (vertical axis), together with the value of $q_{\min} = \min_{x\in[-K_m,K_m]} q(x, 0) = q(K_m, 0) = \sqrt{1 - m}$ (yellow curve) for $m \in (0, 1)$. For the potential (4), $q_{\max} = \max_{x\in[-K_m,K_m]} q(x, 0) = q(0, 0) = 1$. The periodic and antiperiodic eigenvalues of $\mathcal{L}$ along the imaginary z axis were computed using finite truncations of Eqs. (A10) (see Ref. [40] and the Appendix for details). Notice all gaps are closed when $m = 0$ and they open as $m > 0$ and remain open for all $m \in (0, 1)$. In the singular limit $m \to 1$, the band widths

tend to zero, and the periodic and antiperiodic eigenvalues "collide" to form the point spectrum of $\mathcal{L}$ on the line.

Even though $\mathcal{L}$ is not self-adjoint, its spectrum in the limit $\epsilon \to 0$ can be effectively characterized using WKB methods [49,50], which allows one to obtain precise asymptotic estimates for the location of band edges, band widths, and gap widths (see Appendix). The results of the WKB analysis show that all bands lie along the finite segment $\Gamma = (-iq_{\max}, iq_{\max})$ in the complex z-plane. As $\epsilon \to 0$, however, the behavior of bands and gaps in the range $\Gamma_o = (0, iq_{\min})$ differs from those in $\Gamma_g = (iq_{\min}, iq_{\max})$. These two portions of the spectrum are those respectively located below (in white) and above (in gray) the yellow curve in Fig. 2(right) for each value of m. Inside Γ_g, the band widths decay exponentially in ϵ, while the gap widths decay algebraically. Hence, the ratio of band width to gap width tends to zero, and the bands accumulate according to some limiting density $\varphi(z)$ found in Ref. [39] (see the Appendix for details). Conversely, inside Γ_o, it is the relative band gaps that tend to zero [cf. Eq. (A13) in the Appendix], giving rise to a continuous band in the limit. Thus, in the semiclassical limit, the spectrum of the elliptic potential (4) is compatible with the thermodynamic spectral scaling of a SG or a BG [38,39]. As $m \to 1$, the range Γ_o tends to zero, and one gets a pure SG spectrum. Conversely, as $m \to 0$, it is the range Γ_g that tends to zero, and one obtains the spectrum of the soliton condensate. For $0 < m < 1$ we get the spectrum of a BG, which can be interpreted as a "composite," or partially condensed, SG. Next we characterize in detail the statistical properties of this gas.

We can derive the two key quantities in the spectral theory of soliton and breather gases, namely, the density of bands, and the normalized logarithmic band width. In particular, the density of bands $\varphi(z)$ is (see the Appendix for details)

$$\varphi(z) = \frac{2|z|}{\pi} \int_0^{x_o(z)} [\mathrm{dn}^2(x;m) - |z|^2]^{-1/2}\, \mathrm{d}x, \tag{5}$$

where $x_o(z) = K_m$ for $z \in (0, iq_{\min})$ and $x_o(z) > 0$ is a simple turning point [at which $\mathrm{dn}(x;m) = |z|$] for $z \in (iq_{\min}, i)$. (Note that $\int_0^{K_m} \mathrm{dn}(x;m)\, \mathrm{d}x = \pi/2$, which ensures that $\int_0^1 \varphi(z)\, \mathrm{d}|z| = 1$. Note also that for $z \in \Gamma_g$, the above expressions follow directly from the analysis of Ref. [39].)

Following Ref. [39], we can obtain the density of states (DOS) $f(z)$ (see the Appendix for details) $f(z) = \varphi(z)/(2K_m)$. (Note that, strictly speaking, $f(z)$ is a "reduced" DOS. The "full" DOS for the bound-state potential is given by $\tilde{f}(z) = f(\eta)\delta(\xi)$, where $\xi = \mathrm{Re}\, z$, $\eta = \mathrm{Im}\, z$, and $\delta(x)$ is the Dirac δ function; see Ref. [21].)

As $m \to 0$, Γ_g collapses, and $f(\eta)$ tends to the Weyl distribution of a soliton condensate—a critically dense SG (see the Appendix for details). Conversely, as $m \to 1$, $L \to \infty$, Γ_o collapses, and $f(\eta)$ tends to zero, as appropriate for a rarified SG. Thus, as we already mentioned, the BG interpolating between these two extremes, when $0 < m < 1$, can be viewed as a composite SG. The interpretation of a BG as a composite SG is also supported by the results of Ref. [51], where basic fNLS breathers were generated numerically with high accuracy by appropriately configuring N-soliton fNLS solutions with large N.

IV. KURTOSIS AND NUMERICAL VALIDATION

Kurtosis is an important characteristic of a random wave field, indicating its deviation from Gaussianity. With a slight abuse of conventional terminology here we will use the definition of kurtosis κ as the fourth normalized moment of the probability distribution for the wave amplitude $|q|$. With this definition the Gaussian wave field will have $\kappa = 2$; see, e.g., Ref. [52]. The spectral DOS allows one to evaluate the kurtosis of the SG wave field. In Ref. [21], the following general expression for the kurtosis of spatially uniform bound-state SG was obtained:

$$\kappa = \frac{\langle |q|^4 \rangle}{\langle |q|^2 \rangle^2} = \frac{2\overline{\eta^3}}{3\overline{\eta^2}}, \tag{6}$$

where the angle brackets denote ensemble average, $\eta = \mathrm{Im}\, z$, and the overbar, denote average over the DOS,

$$\overline{\eta^k} = \int_\gamma \eta^k f(\eta)\, \mathrm{d}\eta = \frac{c_k}{L} \int_0^L q^{k+1}(x,0)\, \mathrm{d}x, \tag{7}$$

i.e., the moments of the DOS $f(\eta)$, where γ is the spectral support of the SG and where the last equality follows from Ref. [39], with $c_1 = \frac{1}{4}$ and $c_3 = \frac{3}{16}$. Thus,

$$\kappa = 2\kappa_0, \tag{8a}$$

where κ_0 is the normalized fourth moment of the IC, namely,

$$\kappa_0 = L \frac{\int_0^L |q(x,0)|^4\, \mathrm{d}x}{\left(\int_0^L |q(x,0)|^2\, \mathrm{d}x\right)^2}. \tag{8b}$$

This result is consistent with the kurtosis doubling obtained in Ref. [21] for the SG fission from partially coherent waves, with a crucial difference: *here, κ_0 is computed from a purely deterministic IC*. A calculation of the kurtosis for a periodic BG based on the results of Ref. [39] leads to the same expressions (8a) and (8b). Moreover, and importantly, a straightforward analysis of the above expression using Jensen's inequality (see the Appendix for details) allows one to conclude that *any periodic SG or BG of the fNLS equation (1) generated by a deterministic real and even single-lobe potential $q(x,0)$ has kurtosis $\kappa \geqslant 2$. Moroever, $\kappa = 2$ if and only if $q(x,0)$ is constant*. Recall that $\kappa > 2$ implies heavy-tailed non-Gaussian statistics, which is an indication of the possible presence of rogue waves [53–55].

In particular, for the potential (4), a straightforward calculation allows us to obtain the following explicit expression for κ_0:

$$\kappa_0 = K_m[2(2-m)E_m - (1-m)K_m]/\left(3E_m^2\right), \tag{9}$$

where E_m is the complete elliptic integral of the second kind [45].

Next we discuss the numerically computed time evolution of the fNLS solutions produced by the potential (4).

Figure 1 demonstrates how the addition of a small amount of zero-mean white Gaussian noise (with standard deviation $\sigma = 10^{-2}$) to the IC effectively randomizes the solution. Figure 3 (left) shows the temporal evolution of the normalized fourth moment $|q|^4/(|q|^2)^2$ of the resulting fNLS solutions with $\epsilon = 1/20$ and the same amount of white Gaussian noise

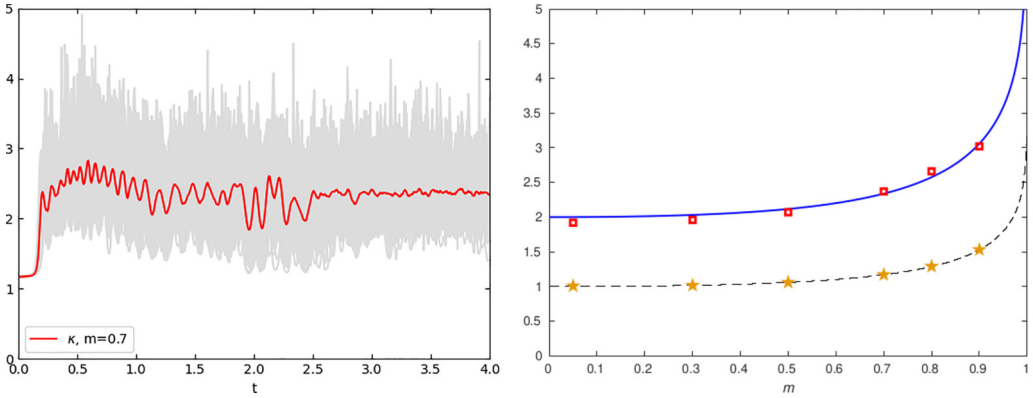

FIG. 3. Left: The averaged temporal evolution of the kurtosis from an ensemble of noise realizations (red line). The gray region shows the envelope of the normalized fourth moment of the solution from all individual noise realizations. Right: The kurtosis of a fully randomized gas as a function of the elliptic parameter m. Blue curve: theoretical prediction from Eqs. (8a) and (9). Dashed black curve: κ_0 from Eq. (9). Red squares: Numerically computed asymptotic value of kurtosis. Yellow stars: Ensemble average of the numerically evaluated integral from Eq. (8b) for ICs consisting of the dn potential plus noise.

as before, as well as their ensemble average (i.e., the kurtosis), clearly demonstrating the establishment of a statistically stationary integrable turbulence state. Finally, Fig. 3 (right) shows how the dependence of the kurtosis on the elliptic parameter m matches the theoretical prediction from Eqs. (6)–(9), providing a strong validation of the analytical predictions.

V. CONCLUDING REMARKS

In summary, we have presented an analytically tractable model describing a mechanism for the formation of integrable turbulence via BG fission of a semiclassical elliptic potential augmented by weak noise. Our analysis introduces a natural interpretation of a BG as a "composite SG," consisting of two distinct components: a regular SG plus a soliton condensate. The analytical model comprises a one-parameter family of such BGs, which interpolates between a pure soliton condensate (as $m \to 0$) and a rarified SG (as $m \to 1$) [56–59]. Intermediate values of m give rise to a mixed regime that interpolates between the above two extremes. We validated the theoretical results with direct numerical simulations of the BG fission and demonstrated the establishment, at large t of a statistically stationary integrable turbulence field characterised by the kurtosis value which is shown analytically and confirmed numerically to be twice as large as the fourth normalized moment of the initial elliptic potential, implying, in particular, the presence of rogue waves for all nonzero values of m.

We expect that similar results will hold for arbitrary real single-lobe periodic potentials. Our results also open up a number of interesting avenues for further research. Since the ZS problem is common to all equations of the AKNS hierarchy, the results of this work will generate SGs/BGs for all such equations, which although spectrally equivalent, exhibit qualitatively different dynamics. The study of their resulting SGs/BGs is threfore an interesting open question. For example, despite some recent work [60,61], the spectral theory of SGs for the focusing modified Korteweg-de Vries (mKdV) equation is still open, and we expect that the mKdV soliton gas phenomenology will be different than that of both the KdV and focusing NLS gases, potentially involving solitons of both polarities in the same gas.

ACKNOWLEDGMENTS

We thank the Isaac Newton Institute for Mathematical Sciences, Cambridge, for support and hospitality during the program Emergent Phenomena in Nonlinear Dispersive Waves, where work on this paper was undertaken. This work was supported by EPSRC Grant No. EP/V521929/1. We also thank Mark Hoefer for useful suggestions. The work of G.B. and A.T. was partially supported by the National Science Foundation under Grants No. DMS-2009487 and No. DMS-2009647, respectively, and that of X.-D.L. by the National Natural Science Foundation of China under Grant No. 12101590. The work of A.T. was also partially supported by a grant from the Simons Foundation.

APPENDIX

In this Appendix we provide some additional details on various results presented in the main text.

Jacobi dn potential and the Lax spectrum. In Ref. [40] we studied the focusing NLS equation

$$iq_t + q_{xx} + 2|q|^2 q = 0, \tag{A1}$$

where the initial condition (IC) is a multiple Jacobi "dn" elliptic function [45]:

$$q(x,0) = A\,\mathrm{dn}(x;m), \quad A \in \mathbb{R}. \tag{A2}$$

As m goes from 0 to 1 the fNLS dynamics corresponding to $N\,\mathrm{dn}(x;m)$ initial data interpolates between plane-wave background ($m = 0$), to genus $2N-1$ finite-gap solution ($0 < m < 1$), to pure N-soliton ($m = 1$).

To connect the above problem to the semiclassical setting, it is sufficient to rescale q and t to make the initial data independent of A, by letting $q(x,t) \mapsto Aq(x,At)$, which yields Eq. (1) with $\epsilon = 1/A$ and $q(x,0)$ given by Eq. (4). Hence, studying the semiclassical limit ($\epsilon \to 0$) of Eq. (1) with IC

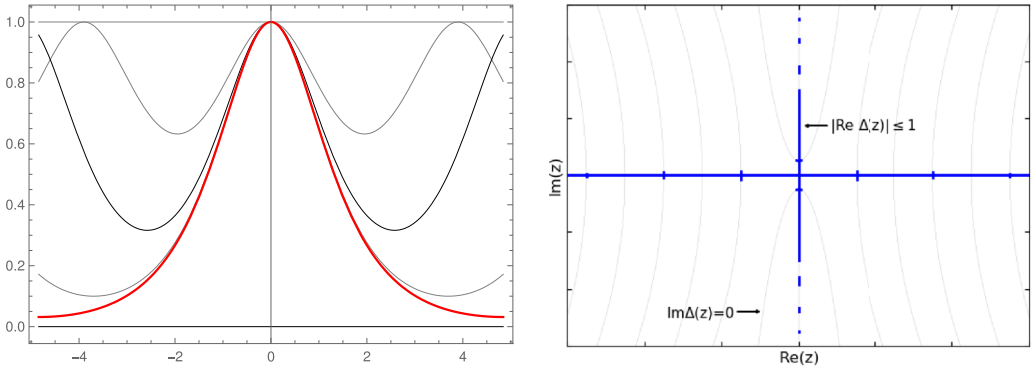

FIG. 4. Left: $\mathrm{dn}(x;m)$ (vertical axis) as a function of x (horizontal axis) for various values of the elliptic parameter m. From top to bottom: $m = 0$ (constant), 0.6 (gray), 0.9 (black), 0.99 (gray) and 0.999 (red). Right: Diagram illustrating the curves $\mathrm{Im}\,\Delta(z) = 0$ (black) and the Lax spectrum $\Sigma(\mathcal{L})$ (blue) in the complex z plane for the potential (4) with generic (noninteger) value of ϵ.

(4) is equivalent to studying the large-A limit of Eqs. (A1) and (A2).

Figure 4(left) depicts the potential (4) for various values of the elliptic parameter $m \in (0, 1)$. Recall that the real period of the dn potential is $2K_m$, where $K_m = K(m)$ is the complete elliptic integral of the first kind [45]. Figure 4(right) shows the contours $\{z : \mathrm{Im}\,\Delta(z) = 0\}$ (thin black curves) together with the Lax spectrum (thick blue curves) for a generic (noninteger) value of the semiclassical parameter ϵ. Figure 5 shows the noise-augmented initial conditions (ICs) for two different values of m and Fig. 6 compares the Lax spectrum with and without noise, demonstrating that the noise does not affect it appreciably. In particular, the number and locations of the solitonic excitations remains unchanged.

In Ref. [40] we proved that the Lax spectrum of the focusing ZS scattering problem associated with Eq. (A1) and dnoidal potential (A2) and $A \in \mathbb{Z}$ is comprised of $2A$ Schwarz-symmetric bands along the imaginary axis of the spectral variable. As a result, the corresponding solutions of focusing NLS are special "finite-gap" solutions of genus $2A - 1$. Next, we provide some details on how the spectrum can be efficiently computed numerically.

PT-symmetric periodic Schrödinger potentials with real spectrum. When the potential is real-valued as with Eq. (4), $\Delta(z)$ also possesses an additional symmetry: $\Delta(-z^*) = \Delta(z)$, and thus the eigenvalues come in quartets, i.e., $\{z, z^*, -z, -z^*\}$. Moreover, the transformation $\mathbf{w} = \Lambda\mathbf{v}$, where $\mathbf{w}(x, \lambda) = (w_+, w_-)^T$ and

$$\Lambda = \frac{1}{\sqrt{2}}\begin{pmatrix} 1 & i \\ 1 & -i \end{pmatrix}, \tag{A3}$$

maps the ZS problem into the time-independent Schrödinger equation with a complex periodic potential, namely,

$$H_\pm w_\pm = \lambda w_\pm, \quad \lambda = z^2, \tag{A4a}$$

where

$$H_\pm = -\epsilon^2\partial_x^2 + V_\pm(x), \quad V_\pm(x) = \mp i\epsilon q_x - q^2. \tag{A4b}$$

Recall that the Schrödinger equation with a periodic potential is referred to as Hill's equation [62]. If q is real and even, then the potentials are PT-symmetric: $V_\pm(-x) = V_\pm^*(x)$. In particular, for the elliptic potential Eq. (4), $H_\pm$ is

$$H_\pm = -\epsilon^2\partial_x^2 - \mathrm{dn}^2(x) \pm i\epsilon m\,\mathrm{sn}(x)\,\mathrm{cn}(x). \tag{A5}$$

Since $\Sigma(H_+) = \Sigma(H_-)$ it is enough to consider only H_-. Below we discuss that, even though $H_\pm$ are not Hermitian, all of their eigenvalues are real.

A further simplification is obtained via the change of variable $y = 2\,\mathrm{am}(x;m)$ [where am is the Jacobi amplitude], which maps Eq. (A5) into a complex perturbation of Ince's

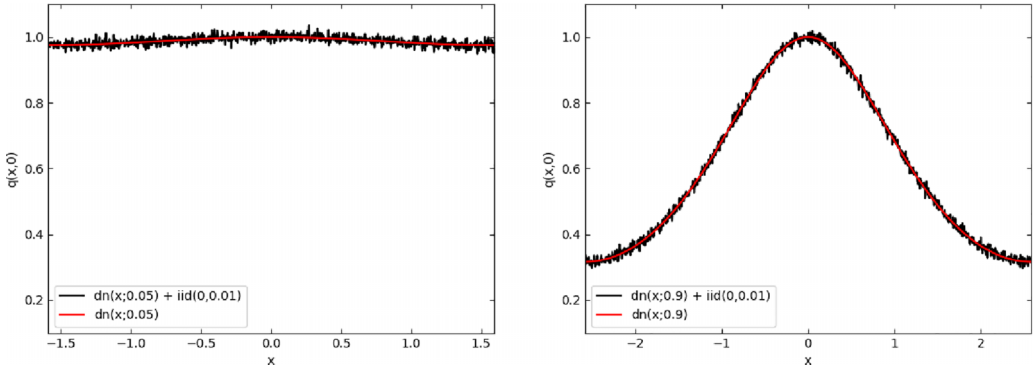

FIG. 5. Red curve: Initial condition (4). Black curve: Same augmented by Gaussian noise with mean $\mu = 0$ and standard deviation $\sigma = 10^{-2}$. Left: $m = 0.05$. Right: $m = 0.9$.

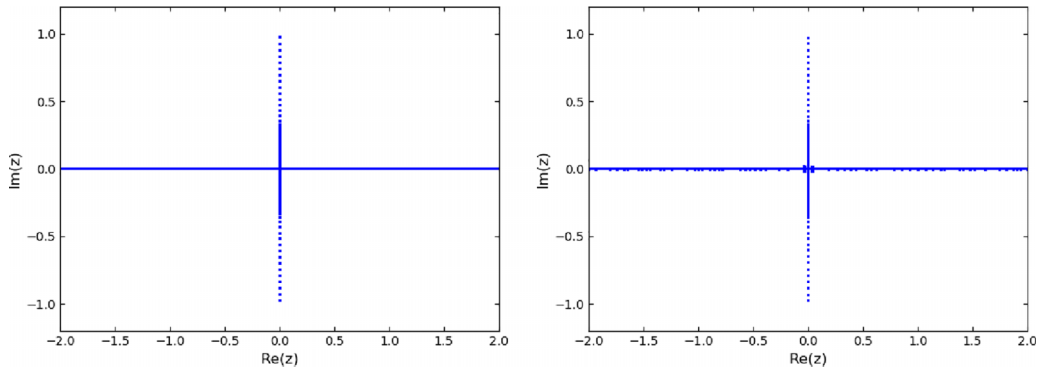

FIG. 6. Left: Numerically computed spectrum of the scattering problem for the dn potential with $m = 0.9$ via the Fourier-Hill method [63]. Right: Same but with noise added to the potential with $\mu = 0$ and $\sigma = 10^{-2}$.

equation [62]:

$$4\epsilon^2[1 - m\sin^2(y/2)]\, w_{yy} - \epsilon^2(m\sin y)\, w_y + \left[\lambda + (1 - m\sin^2(y/2)) + i\epsilon\frac{m}{2}\sin y\right] w = 0. \quad \text{(A6)}$$

Bloch-Floquet theory implies that any bounded solutions of Eq. (A6) can be written as $w(y) = \mathrm{e}^{i\nu y}\, p(y)$, where $\nu \in \mathbb{R}$ is the Floquet exponent and $p(y + 2\pi) = p(y)$, and can therefore be expanded in Fourier series, with Fourier coefficients given by a three-term recurrence relation. The eigenvalues of the ZS problem are then related to the (real or) complex values of λ for which the above ODE admits bounded solutions. Integer and half-integer values of ν yield respectively periodic and antiperiodic eigenfunctions.

Three-term recurrence relation. Any solution of Eq. (A6) that is bounded for all $y \in \mathbb{R}$ can be represented by a Fourier series as

$$w(y;\lambda) = e^{i\nu y}\sum_{n\in\mathbb{Z}} c_n\, e^{iny}, \quad \text{(A7)}$$

with $\nu \in \mathbb{R}$. The coefficients $\{c_n\}_{n\in\mathbb{Z}}$ are given by the three-term recurrence relation

$$\alpha_n c_{n-1} + (\beta_n - \lambda)c_n + \gamma_n c_{n+1} = 0, \quad \text{(A8)}$$

where, for all $n \in \mathbb{Z}$,

$$\alpha_n = -m\left[\tfrac{1}{2} - \epsilon(n + \nu - 1)\right]\left[\tfrac{1}{2} + \epsilon\left(n + \nu - \tfrac{1}{2}\right)\right], \quad \text{(A9a)}$$

$$\beta_n = (1 - m/2)[\epsilon^2(2n + 2\nu)^2 - 1], \quad \text{(A9b)}$$

$$\gamma_n = -m\left[\tfrac{1}{2} - \epsilon(n + \nu + 1)\right]\left[\tfrac{1}{2} + \epsilon\left(n + \nu + \tfrac{1}{2}\right)\right]. \quad \text{(A9c)}$$

Elliptic finite-band potentials. When $\epsilon = 1/N$, some of the coefficents in Eqs. (A9) vanish, and as a result it is possible to decompose the doubly-infinite recurrence relation into two semi-infinite ones. Specifically, let

$$B_o^{\pm} = \begin{pmatrix} \beta_j & \gamma_j & & \\ \alpha_{j+1} & \beta_{j+1} & \gamma_{j+1} & \\ & \ddots & \ddots & \ddots \end{pmatrix}, \quad \text{(A10a)}$$

$$B_\infty^{\pm} = \begin{pmatrix} \beta_{-j} & \alpha_{-j} & & \\ \gamma_{-j-1} & \beta_{-j-1} & \alpha_{-j-1} & \\ & \ddots & \ddots & \ddots \end{pmatrix}, \quad \text{(A10b)}$$

with $\nu = N/2$ and $j = 0$ for the minus sign and $\nu = (1 - N)/2$ and $j = 1$ for the plus sign. The periodic and antiperiodic spectrum of H_- is the union of the spectra of $B_o^{\pm}$ and $B_\infty^{\pm}$. Specifically: when N is even, B_o^- and B_∞^- yield the periodic eigenvalues and B_o^+ and B_∞^+ the antiperiodic ones, and viceversa when N is odd. In Ref. [40] we proved that the eigenvalues of all four of these half-infinite matrices are real. This is the key to prove that, for any $m \in (0, 1)$, the potential q in Eq. (4) for the focusing ZS scattering problem is finite-band if and only if $\epsilon = 1/N$ with $N \in \mathbb{N}$. (The result is easily extended to $N \in \mathbb{Z}$ by phase invariance.) Moreover, if $\epsilon = 1/N$, then q is a $2N$-band potential, and

$$\Sigma(\mathcal{L}) = \mathbb{R} \cup \left(\bigcup_{n=1}^{N}[-i\eta_{2n}, -i\eta_{2n-1}] \cup [i\eta_{2n-1}, i\eta_{2n}]\right), \quad \text{(A11)}$$

where $0 < \eta_1 < \eta_2 < \cdots < \eta_{2N} < 1$. This implies that the spectral curve and the flow induced by each member of the Ablowitz-Kaup-Newell-Segur (AKNS) hierarchy has finite genus $2N - 1$. Importantly, the finite truncations of the matrices (A10) provide an efficient way to numerically compute the spectrum.

Semiclassical WKB analysis of the ZS problem. Next we consider the semiclassical limit of the spectrum, namely the limiting behavior of bands and gaps as $\epsilon \to 0$. It is useful to briefly recall the asymptotic analysis of the focusing ZS scattering problem via WKB methods from Ref. [49]. We emphasize that the results of this and the next few sections apply to a broad class of potentials, not just dn.

Suppose that $q(x)$ is the $2L$-periodic extension of a real, even, nonnegative single-lobe potential. Thus, q has one maximum and one minimum in $(-L, L]$, which without loss of generality can be taken to be respectively at $x = 0$ and $x = L$. To avoid trivial cases, assume that q is not constant. Let

$$q_{\max} = q(0), \quad q_{\min} = q(L), \quad \text{(A12a)}$$

and

$$s(x, z) = \int_{-x_o(z)}^{x} \sqrt{|q^2(u) + z^2|}\, \mathrm{d}u, \quad \text{(A12b)}$$

where $z \in \mathbb{R} \cup i\mathbb{R}$, and $x_o(z)$ is a simple (real) turning point. Without loss of generality we can limit ourselves to considering $\mathrm{Im}\, z \geqslant 0$ thanks to the Schwarz symmetry of the spectrum. Then, as $\epsilon \to 0$ (see Refs. [49,50]):

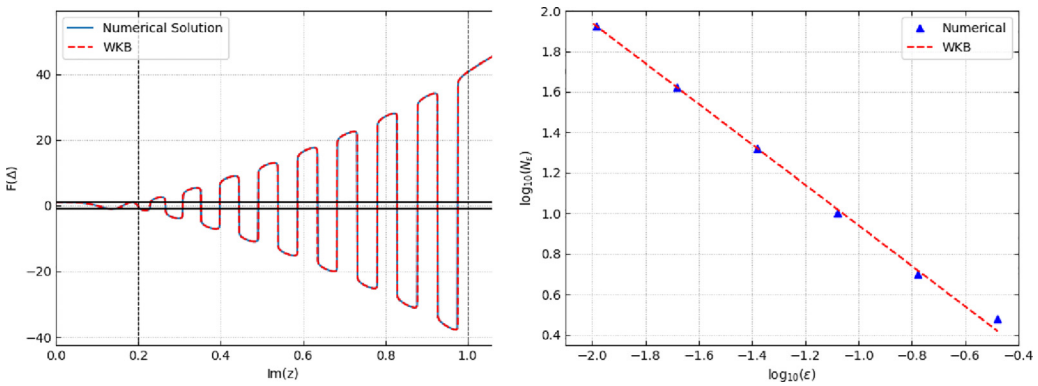

FIG. 7. Left: the numerically computed Floquet discriminant (in blue) for the potential (4) with $m = 0.96$ and $\epsilon = 1/20$, using fourth-order Runge-Kutta versus the WKB approximation (in red). The black solid horizontal lines show $\Delta = \pm 1$. The black dashed vertical lines show $\mathrm{Im}(z) = q_{\min}$ and $\mathrm{Im}(z) = q_{\max}$. Note that, to show the exponentially growing oscillations, the function $F(\tau) = \tau$ for $|\tau| \leqslant 1$ and $F(\tau) = \mathrm{sgn}(\tau)(1 + \log_{10}|\tau|)$ for $|\tau| > 1$ is plotted. Right: The number of spectral bands for $z \in \Gamma_g$ as predicted by WKB (red curve) versus the numerically computed values (blue triangles) as a function of ϵ.

(i) For $z \in \Gamma_o \cup \mathbb{R}$, where $\Gamma_o = (0, iq_{\min})$, one has $q^2(x) + z^2 > 0$ for $x \in (-L, L)$. There are no turning points, and

$$\Delta(z;\epsilon) \sim \cos(s_{\mathrm{i}}(z)/\epsilon), \tag{A13}$$

where $s_{\mathrm{i}}(z) = \int_{-L}^{L} \sqrt{q^2(x) + z^2}\, \mathrm{d}x$. Therefore, in the WKB approximation, this range constitutes a single, continuous spectral band. This range corresponds to the region in white in Fig. 2.

(ii) For $z \in \Gamma_g$, where $\Gamma_g = (iq_{\min}, iq_{\max})$, there are two real symmetric turning points $\pm x_o$, i.e., values at which $q^2(\pm x_o) + z^2 = 0$. In this region (see Fig. 7),

$$\Delta(z;\epsilon) \sim \cos(s_1(z)/\epsilon)\cosh(s_{2,\epsilon}(z)/\epsilon), \tag{A14}$$

where $s_1(z) = s(x_o, z)$ and $s_{2,\epsilon}(z) = \epsilon \ln 2 - 2s(-L, z)$. This range corresponds to the region in gray in Fig. 2.

(iii) For $z \in (iq_{\max}, i\infty)$ one has $q^2(x) + z^2 < 0$ for $x \in (-L, L)$. There are no turning points and

$$\Delta(z;\epsilon) \sim \cosh(s_{\mathrm{ii}}(z)/\epsilon), \tag{A15}$$

where $s_{\mathrm{ii}}(z) = \int_{-L}^{L} \sqrt{-q^2(x) - z^2}\, \mathrm{d}x$.

Figure 7 shows a comparison between the predicted behavior of $\Delta(z, \epsilon)$ and the numerically computed value.

Semiclassical limit of bands and gaps in $\mathbf{\Gamma}_g$. When $z \in (iq_{\min}, iq_{\max})$, Eq. (A14) implies that the bands are approximately centered at the roots $\{z_n\}$ of the equation $s_1(z_n) = (n - \frac{1}{2})\pi\epsilon$. Thus, the asymptotic number of bands for $z \in (iq_{\min}, iq_{\max})$ is

$$N^{\epsilon}_{\mathrm{bands}} \sim \left\lfloor \frac{J_g}{\pi\epsilon} \right\rfloor, \quad \epsilon \to 0, \tag{A16a}$$

where

$$J_g = s_1(iq_{\min}) = \int_{-L}^{L} \sqrt{q^2(x) - q^2_{\min}}\, \mathrm{d}x, \tag{A16b}$$

and $\lfloor \cdot \rfloor$ is the floor function.

Next, consider the limit $\epsilon \to 0$ and $n \to \infty$ satisfying $0 < n\epsilon < J_g/\pi$ and n is the band index. Denote the nth band width as $w^{\epsilon}_n = |z^+_n - z^-_n|$, where $\Delta(z^{\pm}_n) = \pm 1$, respectively. Similarly, denote the nth gap width as $g^{\epsilon}_n = |z^{\pm}_{n+1} - z^{\pm}_n|$. Using $\Delta(z^{\pm}_n) = \pm 1$ together with Eq. (A14), one gets

$$w^{\epsilon}_n \sim \frac{4\epsilon}{|s_1'(z_n)|}\, \mathrm{e}^{-s_{2,\epsilon}(z_n)/\epsilon}, \quad \epsilon \to 0. \tag{A17}$$

Moreover, since $g^{\epsilon}_n \sim |z_{n+1} - z_n|$ and $s_1(z_{n+1}) - s_1(z_n) = \pi\epsilon$ it follows that

$$g^{\epsilon}_n \sim \frac{\pi\epsilon}{|s_1'(\xi_n)|}, \quad \epsilon \to 0, \tag{A18}$$

where $\mathrm{Im}(z_{n+1}) < \mathrm{Im}(\xi_n) < \mathrm{Im}(z_n)$. Finally, the band-to-gap ratio $w^{\epsilon}_n/g^{\epsilon}_n \to 0$ as $\epsilon \to 0$ exponentially fast in this region.

Effective solitons in the fNLS equation. Recall that, for localized potentials (i.e., $q(x,t) \to 0$ rapidly as $|x| \to \infty$), solitons are parameterized by the discrete eigenvalues of the ZS scattering problem. In the periodic problem, nonlinear excitations are considered to be "effective solitons" if the relative band width is less than some small threshold parameter [49,64,65], i.e., if $W_n < \kappa$, where $0 < \kappa \ll 1$ and

$$W^{\epsilon}_n = \frac{w^{\epsilon}_n}{w^{\epsilon}_n + g^{\epsilon}_n}. \tag{A19}$$

Thus, rewriting the relative band width as

$$W^{\epsilon}_n = \frac{w^{\epsilon}_n}{g^{\epsilon}_n}\left(\frac{1}{1 + w^{\epsilon}_n/g^{\epsilon}_n}\right), \tag{A20}$$

one can show that

$$W^{\epsilon}_n \sim \frac{4}{\pi}\, \mathrm{e}^{-s_{2,\epsilon}(z_n)/\epsilon}, \quad \epsilon \to 0. \tag{A21}$$

Note that for $z \in (iq_{\min}, iq_{\max})$ the relative band width W_n is monotonic decreasing. Thus, the effective solitons are confined to the interval

$$z \in (z_s, iq_{\max}) \subset (iq_{\min}, iq_{\max}), \tag{A22}$$

where z_s is the unique solution to $W_n = \kappa$. For $z \in (iq_{\min}, iq_{\max})$ let $s_2(z) = -s(-L, z) \geqslant 0$ (see Eq. (A12b)), then to leading order z_s is given implicitly by

$$s_2(z_s) = \frac{\epsilon}{2} \ln\left(\frac{2}{\pi\kappa}\right), \tag{A23}$$

and the number of effective solitons is given by

$$N_{\text{solitons}} = \left\lfloor \frac{s_1(z_s)}{\pi\epsilon} + \frac{1}{2} \right\rfloor. \tag{A24}$$

Expanding $s_2(z)$ about $z = iq_{\min}$ and evaluating at z_s, for any $\kappa > 0$ it follows that $z_s \to iq_{\min}$ as $\epsilon \to 0$. Thus, in the semiclassical limit the entire interval $(iq_{\min}, iq_{\max})$ is comprised of an infinite ensemble of effective solitons.

Semiclassical limit of bands and gaps in Γ_o. Recall that, when $q = \mathrm{dn}(x; m)$ with $m \in (0, 1)$ and $\epsilon = 1/N$ with $N \in \mathbb{N}$ there are precisely N bands for $z \in (0, iq_{\max})$. Hence, not all bands become effective solitons in the limit $\epsilon \to 0$ (see Fig. 2). For $z \in \Gamma_o$, following similar arguments as for $z \in \Gamma_g$, the WKB approach of Ref. [49] implies

$$w_n^\epsilon = O(\epsilon), \quad \epsilon \to 0. \tag{A25}$$

Thus, at $z_* = iq_{\min} = i\,\mathrm{dn}(K_m; m)$, which is the boundary between the intervals $\Gamma_g = (iq_{\min}, iq_{\max})$ and $\Gamma_o = (0, iq_{\min})$, there is a transition from exponentially decaying band widths (giving rise to a soliton gas), to algebraically decaying band widths (giving rise to a soliton condensate). Thus, we have the physically realistic scenario of a generalized breather gas—namely, a soliton gas on a soliton condensate background, which can equivalently be interpreted as a composite, or partially condensed, SG.

The number of bands with support in Γ_o can be computed by noting that Eq. (A13) holds with exponentially small corrections at $\Delta(z) = \pm 1$. Thus, bands in this region are approximately centered at the roots z_n of the equation $s_i(z_n) = (n - \frac{1}{2})\pi\epsilon$. (The existence of a small gap for each $z_n \in \Gamma_o$ was proven in Ref. [40].) The asymptotic number of bands for $z \in (0, iq_{\min})$ is

$$N_{\text{bands}}^\epsilon \sim \left\lfloor \frac{J_o}{\pi\epsilon} \right\rfloor, \quad \epsilon \to 0, \tag{A26a}$$

where

$$J_o = s_i(0) - s_1(iq_{\min}), \tag{A26b}$$

$$s_i(0) = \int_{-L}^{L} q(x)\,\mathrm{d}x. \tag{A26c}$$

Periodic soliton and breather fNLS gases. The semiclassical WKB asymptotics of the periodic ZS problem from Ref. [49] was utilized in Ref. [39] to introduce periodic fNLS SGs and BGs. They could be viewed as the semiclassical limit of periodic fNLS solutions after a sufficiently long time evolution. Under the assumption of an even, nonnegative, continuous, one-hump $2L$-periodic initial potential $q(x)$ with the maximum value located at $x = 0$, the density of band centers $\varphi(z)$ and the scaled logarithmic band width $\nu(z)$ for a periodic fNLS BG/SG were calculated as

$$\varphi(z) = \frac{|z| \int_0^{q^{-1}(|z|)} \frac{dx}{\sqrt{q^2(x)+z^2}}}{\int_0^L \sqrt{q^2(x) - q_{\min}^2}\,dx},$$

$$\nu(z) = \frac{\pi \int_{q^{-1}(|z|)}^{L} \sqrt{|q^2(x) + z^2|}\,dx}{2\int_0^L \sqrt{q^2(x) - q_{\min}^2}\,dx}, \tag{A27}$$

where $q_{\min} \geqslant 0$ is the minimum of $q(x)$ attained at $x = L$, i.e., $q(L) = q_{\min}$. The case of $q_{\min} > 0$ corresponds to a BG, whereas the case $q_{\min} = 0$ corresponds to a SG. In both SG and BG cases the DOS $f(z)$ was calculated to be $f(z) = r\varphi(z)$, where

$$r = \frac{1}{\pi L} \int_0^L \sqrt{q^2(x) - q_{\min}^2}\,\mathrm{d}x. \tag{A28}$$

The interpretation of a BG as a composite SG can be derived from the results of Ref. [39], where one can observe that the DOS $f(z)$ of a periodic BG ($q_{\min} > 0$) in the region Γ_g coincides in Γ_g with the DOS of SG obtained by replacing $q(x)$ with a modified potential $\hat{q}(x)$ by means of making an infinitesimally narrow cut at $x = L$ that replaces the minimum value of $q(L) = q_{\min}$ by $\hat{q}(L) = 0$. In the region Γ_o, the DOS corresponding to $\hat{q}(x)$ is still given by the expression for $r\varphi(z)$ in Eq. (A28), but where now one has to take $q_{\min} = 0$.

The average conserved quantities I_m, $m = 1, 2, \ldots$, for such gases were rigorously obtained in Ref. [39]. In particular, $I_k = 0$ for any even $k \in \mathbb{N}$, while, for any odd $k \in \mathbb{N}$,

$$I_k = \frac{(-1)^{\frac{k+1}{2}} k d_k}{L} \int_0^L q^{k+1}(x)dx, \tag{A29}$$

where, for any odd value of m, d_m is defined as

$$d_m = -\frac{1}{m}\frac{m!!}{(m+1)!!}. \tag{A30}$$

Spectral characteristics of the composite soliton gas. Recall that the density of bands $\varphi(z)$ and scaled logarithmic band width $\nu(z)$ are two key quantities in the spectral theory of soliton gases. Following Eq. (A27), we have that, for $z \in \Gamma_g$, and the dn potential (4)

$$\varphi(z) = \frac{2|z|}{J} \int_0^{\mathrm{dn}^{-1}(|z|)} \frac{\mathrm{d}x}{\sqrt{\mathrm{dn}^2(x;m) + z^2}}, \tag{A31a}$$

$$\nu(z) = \frac{2\pi}{J} \int_{\mathrm{dn}^{-1}(|z|)}^{K_m} \sqrt{|\,\mathrm{dn}^2(x;m) + z^2|}\,\mathrm{d}x, \tag{A31b}$$

with J is a suitable normalization constant, determined below. Thus we can easily express the spectral scaling function as

$$\sigma(z) = \frac{2\nu(z)}{\varphi(z)}. \tag{A32}$$

TABLE I. Numerical simulation parameters and results, where N_{Fourier} is the number of Fourier modes used, M is the number of simulations (each of which corresponds to an independent noise realization), and T_∞ is the numerically observed approximate thermalization time.

m	κ_o	κ_∞	T_∞	M	N_{Fourier}
0.05	1.007	1.92	4	500	1024
0.3	1.016	1.96	4.5	400	1024
0.5	1.059	2.07	4	400	2048
0.7	1.17	2.37	2.5	200	4096
0.8	1.29	2.66	2.5	200	4096
0.9	1.53	3.022	3.0	400	4096

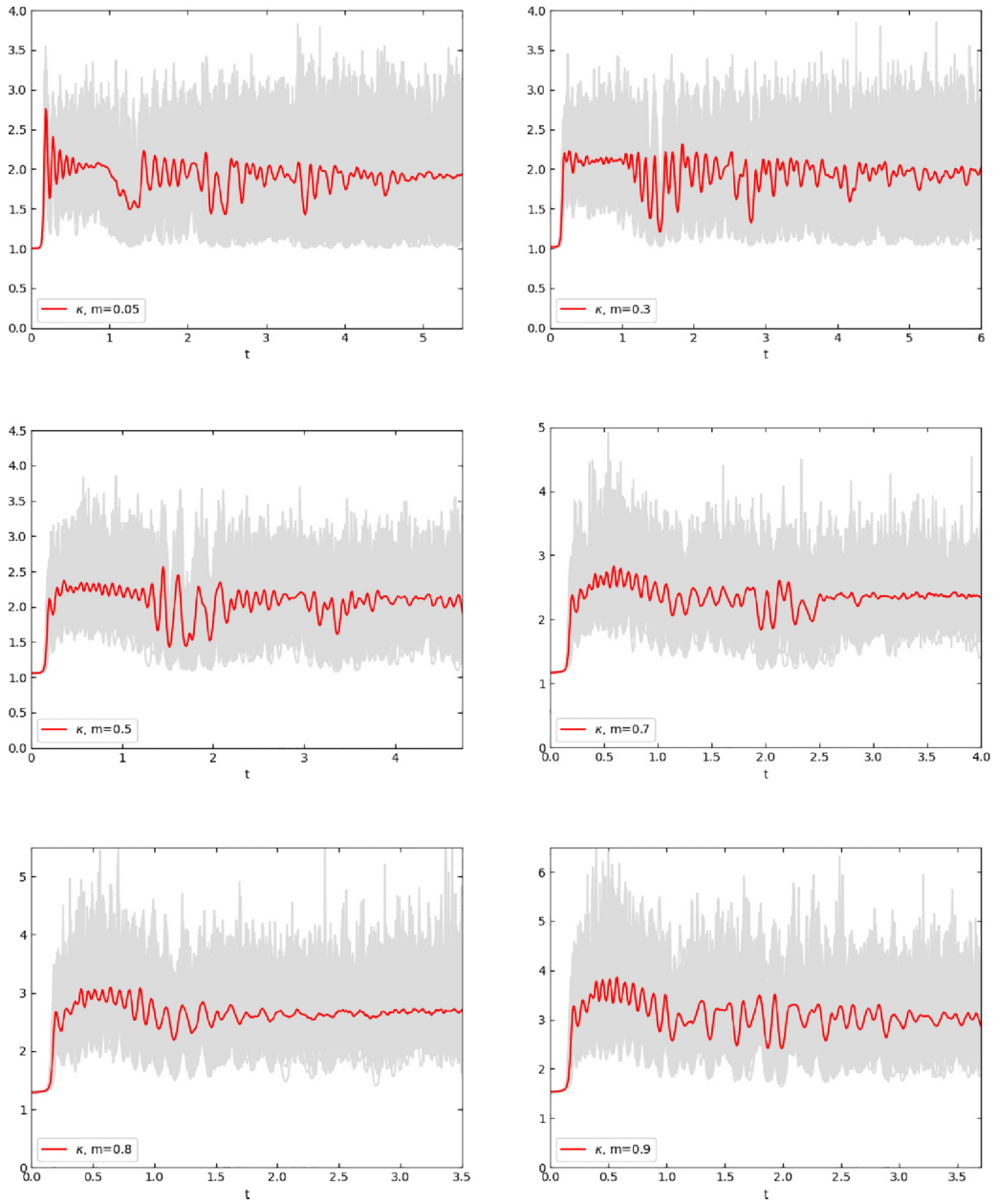

FIG. 8. Time evolution of the kurtosis with $\epsilon = 1/20$ and $\sigma = 10^{-2}$. Gray regions: Envelope of 100 ensemble realizations. Red curves: Ensemble average of M realizations. Top left: $m = 0.05$ ($N = 500$). Top right: $m = 0.3$ ($N = 400$). Middle left: $m = 0.5$ ($N = 400$). Middle right: $m = 0.7$ ($N = 200$). Bottom left: $m = 0.8$ ($N = 200$). Bottom right: $m = 0.9$ ($N = 400$).

Similarly, for $z \in \Gamma_o$, as it was discussed above, we have

$$\varphi(z) = \frac{2|z|}{J} \int_0^{K_m} \frac{\mathrm{d}x}{\sqrt{\mathrm{dn}^2(x;m) + z^2}}, \tag{A33a}$$

$$\sigma(z) = 0. \tag{A33b}$$

(In Γ_o, the spectral scaling function $\sigma(z)$ is zero as required for a condensate.)

Finally, ensuring that the integral of the density of bands $\varphi(z)$ over the whole support $(0, i)$ is one, one can then show that

$$J = J_g + J_o = \int_{-K_m}^{K_m} \mathrm{dn}(x;m)\,\mathrm{d}x = \pi. \tag{A34}$$

Limits $m \to 0$ and $m \to 1$. Next we discuss the density of bands formulas in the limits $m \to 0^+$, and $m \to 1^-$.

Recall that $\mathrm{dn}(x;0) \equiv 1$ and $K(0) = \pi/2$. Thus, $q_{\min} \to 1$ as $m \to 0^+$ and Eq. (A33a) has support $z \in (0, i)$. Moreover, $J_o \to \pi$ as $m \to 0^+$. Thus,

$$\varphi(z) \to \frac{|z|}{\sqrt{1+z^2}}, \quad m \to 0^+, \tag{A35}$$

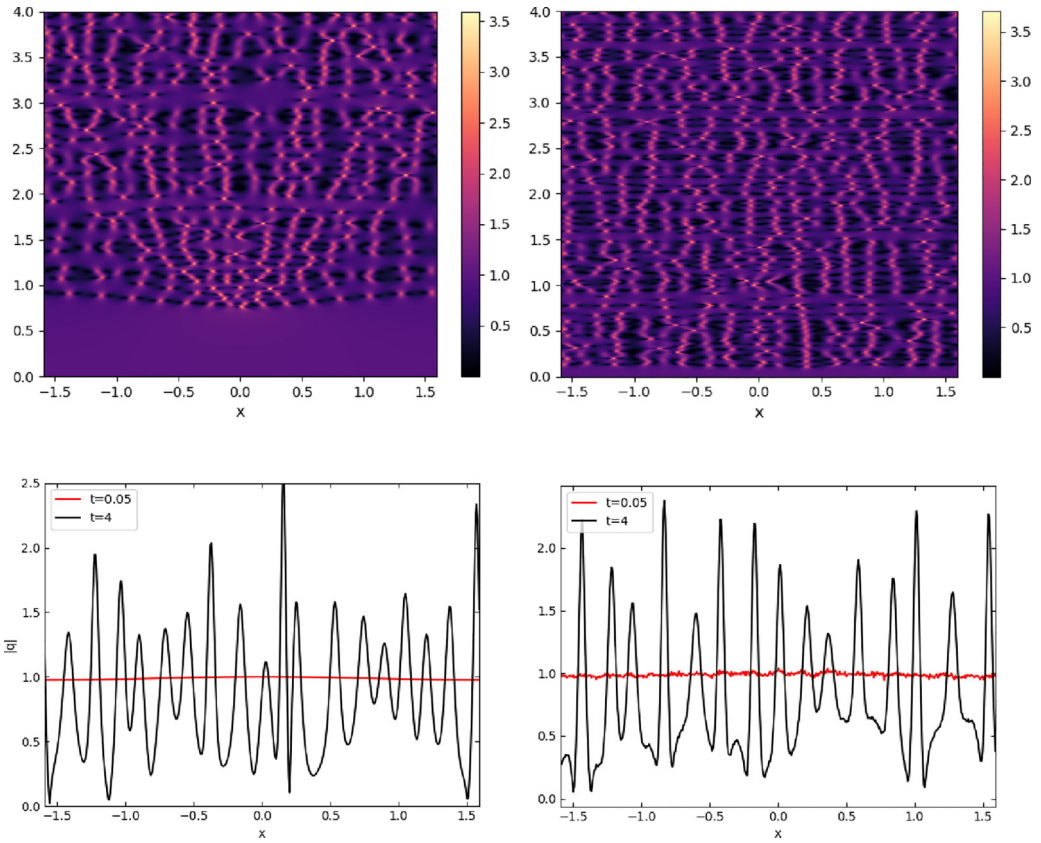

FIG. 9. Numerical solution of the fNLS equation with dn IC, with and without noise, and $\epsilon = 1/20$. Column 1: $\sigma = 0$ (without noise); Column 2: $\sigma = 10^{-2}$ (with noise); Row 1: Density plot, $m = 0.05$; Row 2: Solution at $t = 0.05$ and $t = 4$ for $m = 0.05$. (The randomness in the noiseless simulations is produced by roundoff error accumulation induced by the modulational instability of the fNLS equation, which becomes more and more severe as $\epsilon \to 0$).

which corresponds to Weyl's distribution as expected (see Refs. [33,38]).

Next, recall that $\mathrm{dn}(x;1) \equiv \mathrm{sech}(x)$ and $K(m) \to \infty$ as $m \to 1^-$. Thus, $q_{\min} \to 0$ as $m \to 1^-$ and Eq. (A31a) has support $z \in (0, i)$. Moreover, $J_g \to \pi$ as $m \to 1^-$, and $\mathrm{dn}^{-1}(|z|) \to \mathrm{arcsech}(|z|)$ as $m \to 1^-$. Thus, in this limit we get a uniform distribution:

$$\varphi(z) \to 1, \quad m \to 1^-, \tag{A36}$$

which matches well known results of semiclassical distribution of discrete spectrum for the sech potential [57,59].

Nonlinear dispersion relations. Together with the set $\Gamma_+ = \Gamma_g \cup \Gamma_o$, the spectral scaling function $\sigma(z)$ determines the integral equation (the first nonlinear dispersion relation, NDR) for the DOS $f(z)$ for fNLS SGs:

$$\int_{\Gamma_+} \log\left|\frac{\zeta - z^*}{\zeta - z}\right| f(\zeta)\,\mathrm{d}|\zeta| + \sigma(z) f(z) = \mathrm{Im}\, z. \tag{A37}$$

(Note that in the portion of the spectrum corresponding to a soliton condensate, i.e., Γ_o, one has $\sigma(z) = 0$.) The second NDR involves the spectral flux density, but this quantity is zero in our case since all the nonlinear excitations have zero velocity. It was proven in Ref. [39] that, for periodic SGs and BGs, $f(z) = r\varphi(z)$ solves the first NDR for soliton/breather gases respectively. In the case of the dn potential (4),

$$r = \frac{J}{2\pi L} = \frac{1}{2K_m}. \tag{A38}$$

As a result, expressions (A31a) and (A33a) also yield the DOS $f(z)$ for the dn potential (4).

Kurtosis and Jensen's inequality. In the main text we have shown that the kurtosis κ of a fully developed SG generated by a deterministic real and even periodic single-lobe initial condition $q(x, 0)$ is given by $\kappa = 2\kappa_0$, where

$$\kappa_0 = \frac{L\int_0^L |q(x,0)|^4\,\mathrm{d}x}{\left(\int_0^L |q(x,0)|^2\,\mathrm{d}x\right)^2}. \tag{A39}$$

By employing the rescaling $\tilde{x} = x/L$ and $\tilde{q}(\tilde{x}, 0) = q(L\tilde{x}, 0)$, we can rewrite κ_0 as

$$\kappa_0 = \frac{\int_0^1 |\tilde{q}(\tilde{x},0)|^4\,\mathrm{d}\tilde{x}}{\left(\int_0^1 |\tilde{q}(\tilde{x},0)|^2\,\mathrm{d}\tilde{x}\right)^2}. \tag{A40}$$

Then Jensen's inequality [45] implies that $\kappa_0 \geqslant 1$, with the equality holding only if $q(x, 0)$ is constant.

Numerical methods. We performed several numerical experiments related to the kurtosis of randomly generated solutions to the fNLS equation. In particular, we studied the time evolution of fNLS in the semiclassical limit with elliptic

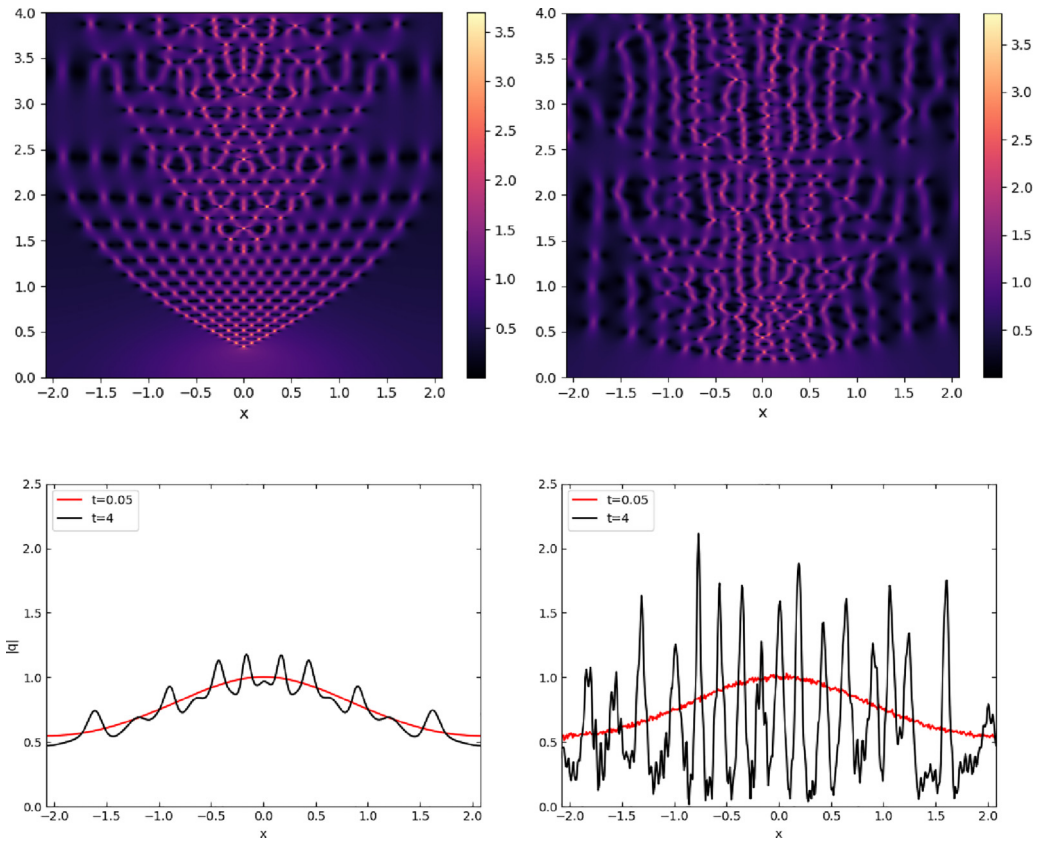

FIG. 10. Same as Fig. 9, but for $m = 0.7$.

IC plus a complex perturbation of independent and identically distributed normal random variables with mean $\mu = 0$ and standard deviation $\sigma = 10^{-2}$.

Due to modulational instability of the fNLS equation, the numerical computation of solutions is a delicate topic, especially in the semiclassical limit. To this end, all the numerical simulations of the fNLS equation (1) presented in this work were performed using an eighth-order split-step method [66]. The spatial and temporal discretization parameters were chosen to be small enough that none of the results presented are affected by numerical errors. Moreover, to ensure numerical accuracy the isospectral property of the scattering data was confirmed at several data points as the simulated solution evolved in time. The Lax spectrum was computed using the Floquet-Fourier-Hill method [63]. Finally, to reduce the number of simulations needed a double-averaging technique was used to compute the kurtosis. That is, at each time the spatial average of $|q|^{2n}$, $n = 1, 2$ was computed, and then the ensemble average was computed.

Further simulation results. For consistency, the numerical experiments presented in this work related to the kurtosis have $\epsilon = 1/20$, and $\sigma = 10^{-2}$ fixed for all values of $m \in (0, 1)$ considered. Table I provides key parameters used in the simulations as well as some of the key quantities related to the kurtosis experiments.

Figure 8 illustrates the time evolution of the fourth normalized moment (i.e., kurtosis) of the solution for $m = 0.05$, 0.3, 0.5, 0.7, 0.8, and 0.9. The gray region is the envelope of 100 ensemble realizations. The red curves are ensemble averages of M realizations. Notice for each m the ensemble average of the kurtosis settles at large times (see Table I for approximate thermalization times).

Finally, to further illustrate the effective thermalization of the SG at large times, Figs. 9–11 show the numerically computed solution of fNLS in the semiclassical limit are provided. In each case, the left column depicts the time evolution of the dn potential (4) while the right column depicts the time evolution of the dn potential (4) with a small complex-valued random perturbation. Further, the top row depicts a density plot while the bottom row depicts the solution at a particular time. In Fig. 9 we have $m = 0.05$ which is a small sinusoidal perturbation of the constant background studied in Ref. [34]. In Fig. 10 $m = 0.7$, and in Fig. 11 $m = 0.9$. Notice the numerically computed solutions with noise are spatially homogeneous at large times.

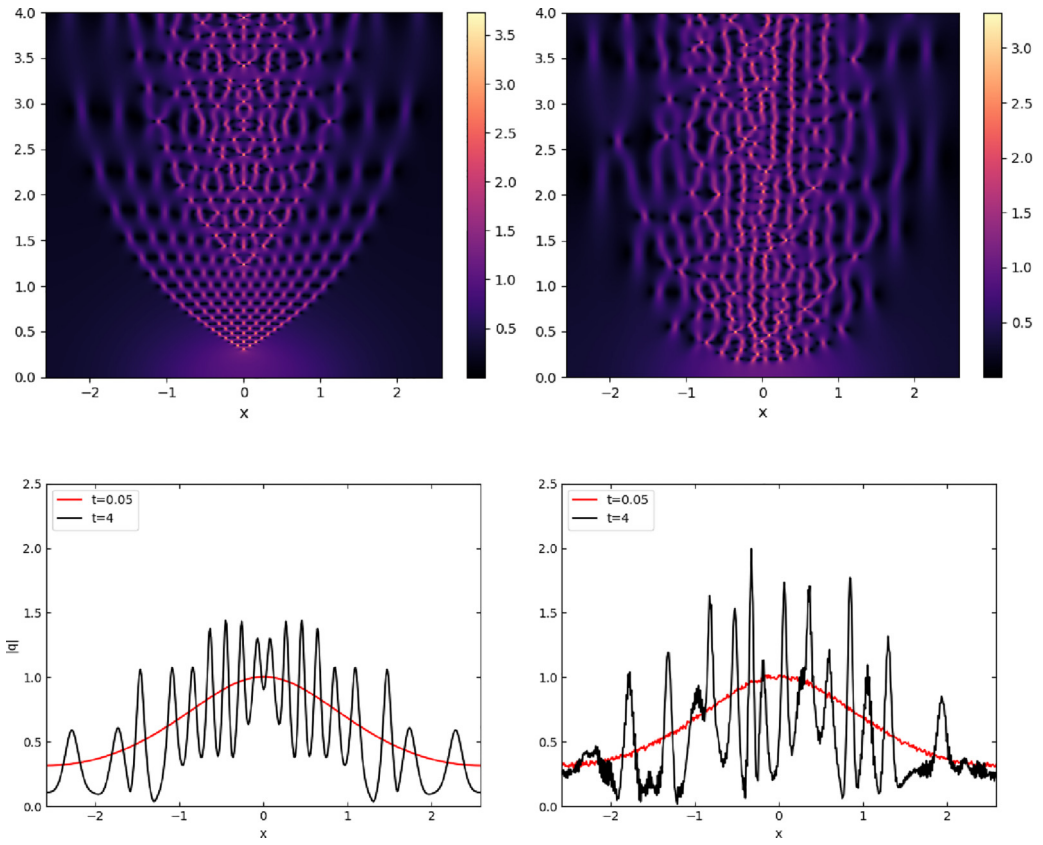

FIG. 11. Same as Fig. 9, but for $m = 0.9$.

[1] M. J. Ablowitz and H. Segur, On the evolution of packets of water waves, J. Fluid Mech. **92**, 691 (1979).

[2] G. P. Agrawal, *Nonlinear Fiber Optics* (Academic Press, New York, NY, 2007).

[3] E. Infeld and G. Rowlands, *Nonlinear Waves, Solitons and Chaos* (Cambridge University Press, Cambridge, UK, 2000).

[4] L. P. Pitaevskii and S. Stringari, *Bose-Einstein Condensation* (Clarendon Press, Oxford, UK, 2003).

[5] M. J. Ablowitz and H. Segur, *Solitons and the Inverse Scattering Transform* (SIAM, Philadelphia, PA, 1981).

[6] S. P. Novikov, S. V. Manakov, L. P. Pitaevskii, and V. E. Zakharov, *Theory of Solitons: The Inverse Scattering Transform* (Plenum, New York, 1984).

[7] L. D. Faddeev and L. A. Takhtajan, *Hamiltonian Methods in the Theory of Solitons* (Springer, Berlin, 1987).

[8] E. D. Belokolos, A. I. Bobenko, V. Z. Enol'skii, A. R. Its, and V. B. Matveev, *Algebro-geometric Approach to Nonlinear Integrable Equations* (Springer-Verlag, Berlin, 1994).

[9] F. Gesztesy and H. Holden, *Soliton Equations and Their Algebro–geometric Solutions, Vol. I* (Cambridge University Press, Cambridge, UK, 2003).

[10] M. J. Ablowitz, B. Prinari, and A. D. Trubatch, *Discrete and Continuous Nonlinear Schrödinger Systems* (Cambridge University Press, Cambridge, UK, 2004).

[11] C. S. Gardner, J. M. Greene, M. D. Kruskal, and R. M. Miura, Method for solving the Korteweg-de Vries equation, Phys. Rev. Lett. **19**, 1095 (1967).

[12] P. D. Lax, Integrals of nonlinear equations of evolution and solitary waves, Commun. Pure Appl. Math. **21**, 467 (1968).

[13] V. E. Zakharov and A. B. Shabat, Exact theory of two-dimensional self-focusing and one-dimensional self-modulation of waves in nonlinear media, Sov. Phys. JETP **34**, 62 (1972).

[14] V. E. Zakharov and A. B. Shabat, Interaction between solitons in a stable medium, Sov. Phys. JETP **37**, 823 (1973).

[15] A. R. Its and V. P. Kotlyarov, Explicit formulas for the solutions of a nonlinear Schroedinger equation, Dokl. Akad. Nauk Ukr. **10**, 965 (1976) [English translation: arXiv:1401.4445 [nlin.si]].

[16] Y.-C. Ma and M. J. Ablowitz, The periodic cubic NLS equation, Stud. Appl. Math. **65**, 113 (1981).

[17] M. G. Forest and J. E. Lee, Geometry and modulation theory for the periodic nonlinear Schrödinger equation, in *Oscillation Theory, Computation, and Methods of Compensated Compactness*, IMA Volumes in Mathematics and Its Applications, edited by C. Dafermos, J. L. Ericksen, D. Kinderlehrer, and M. Slemrod (Springer, New York, NY, 1986), pp. 35–69.

[18] D. W. McLaughlin and E. A. Overman II, *Whiskered Tori for Integrable PDE's: Chaotic Behavior in Near Integrable PDEs*,

Surv. Appl. Math. Vol. I, Ed. J. P. Keller, D. W. McLaughlin, G. P. Papanicolaou (Plenum, New York, NY, 1995).
[19] G. Biondini and G. Kovačič, Inverse scattering transform for the focusing nonlinear Schrödinger equation with nonzero boundary conditions, J. Math. Phys. **55**, 031506 (2014).
[20] V. E. Zakharov, Turbulence in integrable systems, Stud. Appl. Math. **122**, 219 (2009).
[21] T. Congy, G. A. El, G. Roberti, A. Tovbis, S. Randoux, and P. Suret, Statistics of extreme events in integrable turbulence, Phys. Rev. Lett. **132**, 207201 (2024).
[22] G. A. El, Soliton gas in integrable dispersive hydrodynamics, J. Stat. Mech. (2021) 114001.
[23] P. Suret, S. Randoux, A. Gelash, D. Agafontsev, B. Doyon, and G. El, Soliton gas: Theory, numerics, and experiments, Phys. Rev. E **109**, 061001 (2024).
[24] A. Costa, A. R. Osborne, D. T. Resio, S. Alessio, E. Chriví, E. Saggese, K. Bellomo, and C. E. Long, Soliton turbulence in shallow water ocean waves, Phys. Rev. Lett. **113**, 108501 (2014).
[25] I. Redor, E. Barthélemy, H. Michallet, M. Onorato, and N. Mordant, Experimental evidence of a hydrodynamic soliton gas, Phys. Rev. Lett. **122**, 214502 (2019).
[26] P. Suret, A. Tikan, F. Bonnefoy, F. Copie, G. Ducrozet, A. Gelash, G. Prabhudesai, G. Michel, A. Cazaubiel, E. Falcon, G. A. El, and S. Randoux, Nonlinear spectral synthesis of soliton gas in deep-water surface gravity waves, Phys. Rev. Lett. **125**, 264101 (2020).
[27] T. Leduque, E. Barthélemy, H. Michallet, J. Sommeria, N. Mordant, Space-time statistics of 2D soliton gas in shallow water studied by stereoscopic surface mapping, Exp. Fluids **65**, 84 (2024).
[28] G. Marcucci, D. Pierangeli, A. J. Agranat, R.-K. Lee, E. DelRe, and C. Conti, Topological control of extreme waves, Nat. Commun. **10**, 5090 (2019).
[29] A. Schwache and F. Mitschke, Properties of an optical soliton gas, Phys. Rev. E **55**, 7720 (1997).
[30] F. Mitschke, G. Steinmeyer, and A. Schwache, Generation of one-dimensional optical turbulence, Physica D **96**, 251 (1996).
[31] I. Bouchoule and J. Dubail, Generalized hydrodynamics in the one-dimensional Bose gas: Theory and experiments, J. Stat. Mech. (2022) 014003.
[32] S. M. Mossman, G. C. Katsimiga, S. I. Mistakidis, A. Romero-Ros, T. M. Bersano, P. Schmelcher, P. G. Kevrekidis, and P. Engels, Observation of dense collisional soliton complexes in a two-component Bose-Einstein condensate, Commun. Phys. **7**, 163 (2024).
[33] A. Gelash, D. Agafontsev, V. E. Zakharov, G. El, S. Randoux, and P. Suret, Bound state soliton gas dynamics underlying the spontaneous modulational instability, Phys. Rev. Lett. **123**, 234102 (2019).
[34] A. A. Gelash and D. S. Agafontsev, Strongly interacting soliton gas and formation of rogue waves, Phys. Rev. E **98**, 042210 (2018).
[35] V. E. Zakharov, Kinetic equation for solitons, Sov. Phys. JETP **33**, 538 (1971).
[36] G. A. El, The thermodynamic limit of the Whitham equations, Phys. Lett. A **311**, 374 (2003).
[37] G. A. El and A. M. Kamchatnov, Kinetic equation for a dense soliton gas, Phys. Rev. Lett. **95**, 204101 (2005).
[38] G. A. El and A. Tovbis, Spectral theory of soliton and breather gases for the focusing nonlinear Schrödinger equation, Phys. Rev. E **101**, 052207 (2020).
[39] A. Tovbis and F. Wang, Recent developments in spectral theory of the focusing NLS soliton and breather gases: The thermodynamic limit of average densities, fluxes and certain meromorphic differentials; periodic gases, J. Phys. A: Math. Theor. **55**, 424006 (2022).
[40] G. Biondini, X.-D. Luo, J. Oregero and A. Tovbis, Elliptic finite-band potentials of a non-self-adjoint Dirac operator, Adv. Math. **429**, 109188 (2023).
[41] D. S. Agafonstev and V. E. Zakharov, Integrable turbulence and formation of rogue waves, Nonlinearity **28**, 2791 (2015).
[42] D. S. Agafontsev and V. E. Zakharov, Integrable turbulence generated from modulational instability of cnoidal waves, Nonlinearity **29**, 3551 (2016).
[43] G. Roberti, G. El, A. Tovbis, F. Copie, P. Suret, and S. Randoux, Numerical spectral synthesis of breather gas for the focusing nonlinear Schrödinger equation, Phys. Rev. E **103**, 042205 (2021).
[44] D. S. Agafontsev, T. Congy, G. A. El, S. Randoux, G. Roberti, and P. Suret, Spontaneous modulational instability of elliptic periodic waves: the soliton condensate model, arXiv:2411.06922 [nlin.PS].
[45] F. W. Olver, D. W. Lozier, R. F. Boisvert, and C. W. Clark, *NIST Handbook of Mathematical Functions* (Cambridge University Press, Cambridge, UK, 2010).
[46] P. F. Byrd and M. D. Friedman, *Handbook of Elliptic Integrals for Engineers and Scientists* (Springer-Verlag, Berlin, 1971).
[47] J. Satsuma and N. Yajima, Initial value problems of one-dimensional self-modulation of nonlinear waves in dispersive media, Prog. Theor. Phys. Suppl. **55**, 284 (1974).
[48] F. Gesztesy and R. Weikard, A characterization of of all elliptic algebro-geometric solutions of the AKNS hierarchy, Acta Math. **181**, 63 (1998).
[49] G. Biondini and J. Oregero, Semiclassical dynamics and coherent soliton condensates in self-focusing nonlinear media with periodic initial conditions, Stud. Appl. Math. **145**, 325 (2020).
[50] G. Biondini, J. Oregero, and A. Tovbis, On the spectrum of the periodic focusing Zakharov-Shabat operator, J. Spectr. Theory **12**, 939 (2022).
[51] D. Agafontsev, A. Gelash, S. Randoux and P. Suret, Multi-soliton interactions approximating the dynamics of breather solutions, Stud. Appl. Math. **152**, 810 (2024).
[52] R. El Koussaifi, A. Tikan, A. Toffoli, S. Randoux, P. Suret, and M. Onorato, Spontaneous emergence of rogue waves in partially coherent waves: A quantitative experimental comparison between hydrodynamics and optics, Phys. Rev. E **97**, 012208 (2018).
[53] M. Onorato, S. Residori, U. Bortolozzo, A. Montina and F. T. Arecchi, Rogue waves and their generating mechanisms in different physical contexts, Phys. Rep. **528**, 47 (2013).
[54] P. Walczak, S. Randoux, and P. Suret, Optical rogue waves in integrable turbulence, Phys. Rev. Lett. **114**, 143903 (2015).
[55] F. Copie, S. Randoux and P. Suret, The physics of the one-dimensional nonlinear Schrödinger equation in fiber optics: Rogue waves, modulation instability and self-focusing phenomena, Rev. Phys. **5**, 100037 (2020).

[56] S. Venakides, The zero dispersion limit of the Korteweg-de Vries equation with periodic initial data, Trans. AMS **301**, 189 (1987).

[57] S. Kamvissis, K. D. T-R McLaughlin, and P. Miller, *Semiclassical Soliton Ensembles for the Focusing Nonlinear Schrödinger Equation* (Princeton University Press, Princeton, NJ, 2003).

[58] N. M. Ercolani, S. Jin, C. D. Levermore, and W. D. MacEvoy, Jr., The zero-dispersion limit for the odd flows in the focusing Zakharov-Shabat hierarchy, Int. Math. Res. Not. **2003**, 2529 (2003).

[59] A. Tovbis, S. Venakides, and X. Zhou, On semiclassical (zero dispersion limit) solutions of the focusing nonlinear Schrödinger equation, Commun. Pure Appl. Math. **57**, 877 (2004).

[60] E. G. Shurgalina and E. N. Pelinovsky, Nonlinear dynamics of a soliton gas: Modified Korteweg-de Vries equation framework, Phys. Lett. A **380**, 2049 (2016).

[61] M. Girotti, T. Grava, R. Jenkins, K. D. T-R McLaughlin, and A. Minakov, Soliton versus the gas: Fredholm determinants, analysis, and the rapid oscillations behind the kinetic equation, Commun. Pure Appl. Math. **76**, 3233 (2023).

[62] W. Magnus and S. Winkler, *Hill's Equation* (Dover, New York, NY, 1966).

[63] B. Deconinck and J. N. Kutz, Computing spectra of linear operators using the Floquet-Fourier-Hill method, J. Comput. Phys. **219**, 296 (2006).

[64] S. Trillo, G. Deng, G. Biondini, M. Klein, G. F. Clauss, A. Chabchoub, and M. Onorato, Experimental observation and theoretical description of multisoliton fission in shallow water, Phys. Rev. Lett. **117**, 144102 (2016).

[65] A. R. Osborne and L. Bergamasco, The solitons of Zabusky and Kruskal revisited: Perspective in terms of the periodic spectral transform, Physica D **18**, 26 (1986).

[66] H. Yoshida, Construction of high order symplectic integrators, Phys. Lett. A **150**, 262 (1990).